MOLECULAR AND CELLULAR BIOLOGY, Feb. 2010, p. 1059–1066 Vol. 30, No. 4
0270-7306/10/$12.00 doi:10.1128/MCB.01498-09


# Telomere Protection by TPP1 Is Mediated by POT1a and POT1b[▽]

Tatsuya Kibe,[1] Gail A. Osawa,[2] Catherine E. Keegan,[2] and Titia de Lange[1]*

*The Rockefeller University, 1230 York Avenue, New York, New York 10065,[1] and Departments of Pediatrics and Human Genetics, University of Michigan, Ann Arbor, Michigan 48109[2]*

Received 17 November 2009/Returned for modification 25 November 2009/Accepted 30 November 2009

**Mammalian telomeres are protected by the shelterin complex, which contains single-stranded telomeric DNA binding proteins (POT1a and POT1b in rodents, POT1 in other mammals). Mouse POT1a prevents the activation of the ATR kinase and contributes to the repression of the nonhomologous end-joining pathway (NHEJ) at newly replicated telomeres. POT1b represses unscheduled resection of the 5′-ended telomeric DNA strand, resulting in long 3′ overhangs in POT1b KO cells. Both POT1 proteins bind TPP1, forming heterodimers that bind to other proteins in shelterin. Short hairpin RNA (shRNA)-mediated depletion had previously demonstrated that TPP1 contributes to the normal function of POT1a and POT1b. However, these experiments did not establish whether TPP1 has additional functions in shelterin. Here we report on the phenotypes of the conditional deletion of TPP1 from mouse embryo fibroblasts. TPP1 deletion resulted in the release of POT1a and POT1b from chromatin and loss of these proteins from telomeres, indicating that TPP1 is required for the telomere association of POT1a and POT1b but not for their stability. The telomere dysfunction phenotypes associated with deletion of TPP1 were identical to those of POT1a/POT1b DKO cells. No additional telomere dysfunction phenotypes were observed, establishing that the main role of TPP1 is to allow POT1a and POT1b to protect chromosome ends.**

Mammalian cells solve the chromosome end protection problem through the binding of shelterin to the telomeric TTAGGG repeat arrays at chromosome ends (5). Shelterin contains two double-stranded telomeric DNA binding proteins, TRF1 and TRF2, which both interact with the shelterin subunit TIN2. These three shelterin components, as well as the TRF2 interacting factor Rap1, are abundant, potentially covering the majority of the TTAGGG repeat sequences at chromosome ends (30). TIN2 interacts with the less abundant TPP1/POT1 heterodimers and is thought to facilitate the recruitment of the single-stranded telomeric DNA binding proteins to telomeres (15, 21, 35).

Shelterin represses the four major pathways that threaten mammalian telomeres (6). It prevents activation of the ATM and ATR kinases, which can induce cell cycle arrest in response to double-strand breaks (DSBs). Shelterin also blocks the two major repair pathways that act on DSBs: nonhomologous end joining (NHEJ) and homology-directed repair (HDR). Removal of individual components of shelterin leads to highly specific telomere dysfunction phenotypes, allowing assignment of shelterin functions to each of its components.

The POT1 proteins are critical for the repression of ATR signaling (20). Concurrent deletion of POT1a and POT1b from mouse embryo fibroblasts (POT1a/b DKO cells [12]) activates the ATR kinase at most telomeres, presumably because the single-stranded telomeric DNA is exposed to RPA. POT1a/b DKO cells also have a defect in the structure of the telomere terminus, showing extended 3′ overhangs that are thought to be due to excessive resection of the 5′-ended strand in the absence of POT1b (11–13). The combination of these two phenotypes, activation of the ATR kinase and excess single-stranded telomeric DNA, is not observed when either TRF1 or TRF2 is deleted.

In contrast to the activation of ATR signaling in POT1a/b DKO cells, TRF2 deletion results in activation of the ATM kinase at telomeres (3, 16, 20). In addition, TRF2-deficient cells show widespread NHEJ-mediated telomere-telomere fusions (3, 31). This phenotype is readily distinguished from the consequences of POT1a/b loss. POT1a/b DKO cells have a minor telomere fusion phenotype that primarily manifests after DNA replication, resulting in the fusion of sister telomeres (12). In TRF2-deficient cells, most telomere fusions take place in $G_1$ (18), resulting in chromosome-type telomere fusions in the subsequent metaphase. Chromosome-type fusions also occur in the POT1a/b DKO setting, but they are matched in frequency by sister telomere fusions.

The type of telomere dysfunction induced by TRF1 loss is also distinct. Deletion of TRF1 gives rise to DNA replication problems at telomeres that activate the ATR kinase in S phase and leads to aberrant telomere structures in metaphase (referred to as "fragile telomeres") (28). This fragile telomere phenotype is not observed upon deletion of POT1a and POT1b, and the activation of the ATR kinase at telomeres in POT1a/b DKO cells is not dependent on the progression through S phase (Y. Gong and T. de Lange, unpublished data). Furthermore, deletion of TRF1 does not induce excess single-stranded DNA.

These phenotypic distinctions bear witness to the separation of functions within shelterin and also serve as a guide to understanding the contribution of the other shelterin proteins, including TPP1. TPP1 is an oligonucleotide/oligosaccharide-binding fold (OB fold) protein in shelterin that forms a heterodimer with POT1 (32). TPP1 and POT1 are distantly related to the TEBPα/β heterodimer, which is bound to

* Corresponding author. Mailing address: Laboratory for Cell Biology and Genetics, The Rockefeller University, 1230 York Avenue, New York, NY 10065-6399. Phone: (212) 327-8146. Fax: (212) 327-7147. E-mail: delange@mail.rockefeller.edu.

▽ Published ahead of print on 7 December 2009.

telomeric termini of certain ciliates (2, 32, 33). Several lines of evidence indicate that TPP1 mediates the recruitment of POT1 to telomeres. Mammalian TPP1 was discovered based on its interaction with TIN2, and diminished TPP1 levels affect the ability of POT1 to bind to telomeres and protect chromosome ends (14, 15, 21, 26, 33, 35). Since TPP1 enhances the *in vitro* DNA binding activity of POT1 (32), it might mediate the recruitment of POT1 through improving its interaction with the single-stranded telomeric DNA. However, POT1 does not require its DNA binding domain for telomere recruitment, although this domain is critical for telomere protection (23, 26). Thus, it is more likely that the TPP1-TIN2 interaction mediates the binding of POT1 to telomeres. However, POT1 has also been shown to bind to TRF2 *in vitro*, and this interaction has been suggested to constitute a second mechanism for the recruitment of POT1 to telomeres (1, 34).

TPP1 has been suggested to have additional functions at telomeres. Biochemical data showed that TPP1 promotes the interaction between TIN2, TRF1, and TRF2 (4, 25). Therefore, it was suggested that TPP1 plays an essential organizing function in shelterin, predicting that its deletion would affect TRF1 and TRF2 (25). Furthermore, cytogenetic data on cells from the adrenocortical dysplasia (Acd) mouse strain, which carries a hypomorphic mutation for TPP1 (14), revealed complex chromosomal rearrangements in addition to telomere fusions, leading to the suggestion that TPP1 might have additional telomeric or nontelomeric functions (9).

In order to determine the role of TPP1 at telomeres and possibly elsewhere in the genome, we generated a conditional knockout setting in mouse embryo fibroblasts. The results indicate that the main function of TPP1 is to ensure the protection of telomeres by POT1 proteins. Each of the phenotypes of TPP1 loss was also observed in the POT1a/b DKO cells. No evidence was found for a role of TPP1 in stabilizing or promoting the function of other components of shelterin. Furthermore, the results argue against a TPP1-independent mode of telomeric recruitment of POT1.

## MATERIALS AND METHODS

**TPP1 gene targeting.** The *TPP1* targeting construct was made by bacterial artificial chromosome (BAC) recombineering as previously described (22). Briefly, a 6.9-kb genomic fragment containing the *TPP1* gene (official gene name, *Acd*), 2.4 kb of 5′ flanking DNA, and 1.5 kb of 3′ flanking DNA was subcloned into the PL253 vector using the gap repair method (22; http://recombineering.ncifcrf.gov/). PCR primers containing 50 to 70 bp of sequence from intron 2 of the *TPP1* gene were used to amplify the neomycin gene flanked by *loxP* sites from the PL452 vector (22). An EcoRI site was engineered just 5′ of the first *loxP* site for use as a diagnostic restriction site for the targeted allele. This neomycin cassette was inserted into the second intron of the *TPP1* gene using homologous recombination. Following arabinose-induced Cre recombinase expression in EL350 cells (22), the neomycin gene was removed from the construct, leaving the EcoRI site and single *loxP* site within the second intron. A second neomycin cassette was generated by PCR using primers containing 50 to 70 bp of sequence from the eighth intron of the *TPP1* gene to amplify the neomycin gene (flanked by one *loxP* site and two *frt* sites) from the PL451 vector (22). This neomycin cassette was then inserted into the eighth intron of the *TPP1* gene in reverse orientation using homologous recombination. The integrity of both neomycin cassettes was verified by DNA sequence analysis prior to insertion into the targeting vector, and the position and sequence of the upstream *loxP* site and neomycin cassette were verified in the final targeting vector by DNA sequence analysis prior to electroporation into ES cells. Gene targeting in (129S6/SvEvTac × C57BL/6Ncr)-derived G4 mouse embryonic stem cells (10) was performed as described previously (17) with the use of ESGRO (Millipore). Embryonic stem cell clones were screened for the presence of the correctly targeted allele by Southern blotting. Following digestion with EcoRI, 5′ and 3′ probes detected an endogenous 19.8-kb fragment. In the presence of a correctly targeted allele, an 11-kb fragment was detected with the 5′ probe, and a 10.6-kb fragment was detected with the 3′ probe. Using this screening strategy, 11 homologous recombinants were identified that were positive with both the 5′ and 3′ flanking probes. One euploid cell line was injected into B6-albino [B6(Cg)-Tyr$^{c-2J}$/J] blastocysts, and five male chimeric mice were identified. These male chimeras were backcrossed to B6-albino mice, and three out of the five mice produced pups that had transmitted the *TPP1*$^{Floxneo}$ allele through the germ line. Mice carrying the *TPP1*$^{Flox}$ allele (hereinafter *TPP1*$^{F}$) were generated by breeding *TPP1*$^{Floxneo}$ mice to FLPe deleter mice (27). *TPP1*$^{F/+}$ mice were also bred to Cre deleter (EIIa-Cre) mice, resulting in *TPP1*$^{Del/+}$ mice, which carry a deletion of exons 3 to 8.

**Cell culture and retroviral infection.** Mouse embryonic fibroblasts (MEFs) were isolated from E13.5 embryos and cultured in Dulbecco modified Eagle medium (DMEM) supplemented with 1 mM Na pyruvate, 100 U/ml penicillin, 0.1 μg/ml streptomycin, 0.2 mM L-glutamine, 0.1 mM nonessential amino acids, and 15% (vol/vol) fetal calf serum (FCS). MEFs were immortalized by retroviral infection with pBabeSV40-LT (a gift from Greg Hannon) and cultured in media with 10% FCS without sodium pyruvate. Cre recombinase was introduced using Hit&Run-Cre (29) as described previously (3). Short hairpin RNAs (shRNAs) for ATM (sh1, GGAAGTCAAGGAACAACAACTA) and ATR (sh3-1, GGA GATGCAACTCGTTTAA [20]) were introduced using pSuperior-hygromycin retroviral vector and pSuper-puromycin. Luciferase shRNA was used as a negative control. Hygromycin (90 μg/ml) and puromycin (2 μg/ml) selection was applied for 2 days. Full-length mouse TPP1 was expressed from pLPC-myc-puro retroviral expression vector by three retroviral infections at 12-h intervals, and puromycin selection was for 3 days.

**Senescence-associated β-galactosidase staining.** Senescence-associated (SA)-β-galactosidase staining was performed as described previously (8). *TPP1*$^{F/F}$ and *TPP1*$^{F/+}$ simian virus 40 (SV40)-LT-immortalized MEFs were infected with Hit&Run-Cre and cultured for 10 days. On day 10, cells were fixed with 2% formaldehyde-0.2% glutaraldehyde in phosphate-buffered saline (PBS) for 5 min at room temperature and washed twice with PBS. Cells were incubated with staining solution (1 mg/ml 5-bromo-4-chloro-3-indolyl β-galactosidase [X-Gal], 40 mM citric acid-sodium phosphate, pH 6.0, 150 mM NaCl, 2 mM $MgCl_2$, 5 mM potassium ferrocyanide, 5 mM potassium ferricyanide) overnight at 37°C, washed twice with PBS, and photographed.

**Immunoblotting.** Cells were lysed in 2× Laemmli buffer (100 mM Tris-HCl, pH 6.8, 200 mM dithiothreitol [DTT], 3% SDS, 20% glycerol, 0.05% bromophenol blue), denatured for 5 min at 100°C or for 10 min at 80°C (for ATM and ATR), and sheared with an insulin needle or by sonication. Proteins were resolved on SDS-PAGE (5% for ATM and ATR, 8% for POT1a and POT1b, and 10% for other proteins) and transferred to either nitrocellulose or polyvinylidene difluoride (PVDF) (for ATM). Membranes were blocked in PBS or Tris-buffered saline (TBS) with 5% nonfat dry milk and 0.1% Tween 20 for 30 min at room temperature and incubated with the following primary antibodies in PBS or TBS with 5% milk and 0.1% Tween 20 overnight at 4°C: TRF2 (1254), γ-tubulin (GTU 88; Sigma), α-tubulin (Clone B-5-1-2; Sigma), Chk1 S345-P (Cell Signaling Technology), Chk1 (Santa Cruz), Chk2 (BD, Franklin Lakes, NJ), ATM (MAT3; Sigma), ATR (N-19) (Santa Cruz), and Myc 9B11 (Cell Signaling Technology). Immunoblotting for POT1a and POT1b was performed using the renaturation protocol described previously (12) with antibodies 1221 to POT1a and 1223 to POT1b. Membranes were developed with enhanced chemiluminescence (ECL; Amersham).

**ChIP assay.** A chromatin immunoprecipitation (ChIP) assay was performed as described previously (18, 23). At 96 h after Cre infection, cells were cross-linked with 2% paraformaldehyde on a dish for 30 min at room temperature, followed by chelating with glycine, washes with cold PBS, and trypsinization followed by inactivation with serum. Cells were scraped, washed with cold PBS twice, resuspended in cold lysis buffer consisting of 5 mM PIPES [piperazine-*N*,*N*′-bis(2-ethanesulfonic acid)], pH 8.0, 85 mM KCl, 0.5% NP-40, 1 mM phenylmethylsulfonyl fluoride (PMSF), 1 mM DTT, and complete protease inhibitor cocktail and incubated for 10 min on ice. The lysates were sonicated and centrifuged at 13,200 rpm for 10 min at 4°C. The supernatants were diluted with IP dilution buffer (20 mM Tris-HCl, pH 8.0, 150 mM NaCl, 2 mM EDTA, 1% Triton X-100, 0.1% SDS, 1 mM PMSF, 1 mM DTT, complete protease inhibitor cocktail) and used for IPs. The following rabbit polyclonal antibodies were used as crude sera: TRF1 (644), TRF2 (1254), Rap1 (1253), TIN2 (1447), POT1a (1221), and POT1b (1223). Precipitated DNA was washed, extracted, blotted, and hybridized with TTAGGG repeat probe to detect telomeric DNA.

**Cell fractionation.** Cell fractionation was performed as described previously (24). Cells were trypsinized, suspended in media with 10% FCS, collected by centrifugation, washed with PBS, and centrifuged. Cells were resuspended in

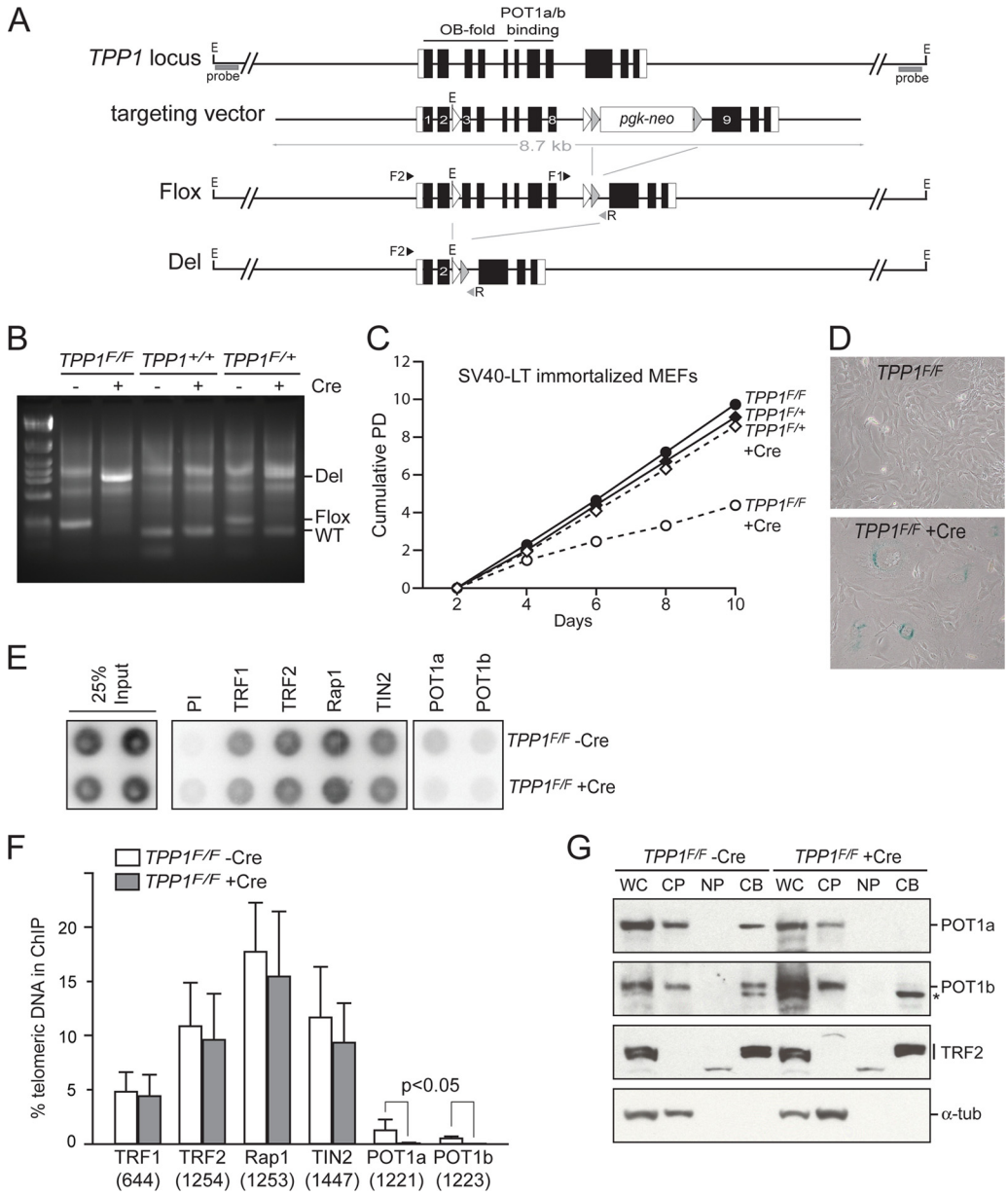


FIG. 1. Conditional deletion of *TPP1* removes POT1a and -b from telomeres. (A) Schematic of the mouse *TPP1*/*Acd* locus on chromosome 8, the targeting vector, the conditional allele ($TPP1^{F}$), and the null allele ($TPP1^{Del}$). PCR primers (F1, F2, and R) and probes for analysis of genomic DNA are indicated. E, EcoRI. (B) PCR analysis of genomic DNA isolated from SV40-LT-immortalized $TPP1^{F/F}$ MEFs at 96 h after Hit&Run-Cre infection. (C) Graph of the proliferation of the indicated MEFs with and without Cre infection. (D) Phase-contrast micrographs of $TPP1^{F/F}$ MEFs at 10 days after Cre infection and the uninfected control. Cells were stained for SA-β-galactosidase. (E) ChIP with shelterin components in *TPP1* KO cells. $TPP1^{F/F}$ MEFs were fixed and analyzed at 96 h after Cre or mock infection. Crude sera were used for the IPs. Telomeric DNA was detected with a TTAGGG repeat probe. Sera used for IPs were the same as in panel F. PI, preimmune. (F) Quantification of the ChIP shown in panel E. Bars show average results of three or four independent experiments and standard deviations. The *P* value was derived from the Wilcoxon rank sum test. PI background ChIP values were subtracted from the other ChIP values. (G) $TPP1^{F/F}$ cells were fractionated prior to or at 96 h after infection with Cre. Whole-cell lysate (WC), cytoplasmic proteins (CP), nucleoplasmic proteins (NP), and chromatin-bound proteins (CB) were analyzed by immunoblotting. α-Tubulin was used as a control for cytoplasmic proteins. Asterisk, nonspecific band.

buffer A (10 mM HEPES, pH 7.9, 10 mM KCl, 1.5 mM $MgCl_2$, 0.34 M sucrose, 10% glycerol, 1 mM DTT, 1 mM PMSF, complete protease inhibitors). Triton X-100 was added, and the mixture was then incubated for 10 min on ice and centrifuged at 1,300 × *g* at 4°C for 4 min. The supernatants were collected as cytoplasmic fractions. The pellets were washed with buffer A, resuspended in buffer B [3 mM EDTA, 0.2 mM ethylene glycol-bis(β-aminoethyl ether)-*N*,*N*,*N*′,*N*′-tetraacetic acid (EGTA), 1 mM DTT, 1 mM PMSF, complete protease inhibitors], and incubated for 30 min on ice. The supernatants (soluble nuclear fraction) were separated from the pellets (chromatin fraction) by centrifugation at 1,700 × *g* at 4°C.

**IF-FISH.** Immunofluorescent fluorescence in situ hybridization (IF-FISH) to detect telomere dysfunction-induced foci (TIFs) was performed as described previously (7). Cells grown on coverslips were fixed for 10 min in 2% paraformaldehyde at room temperature, followed by three 5-min washes with PBS and incubation in blocking solution (1 mg/ml bovine serum albumin [BSA], 3% goat serum, 0.1% Triton X-100, 1 mM EDTA in PBS) for 30 min. Primary antibod-

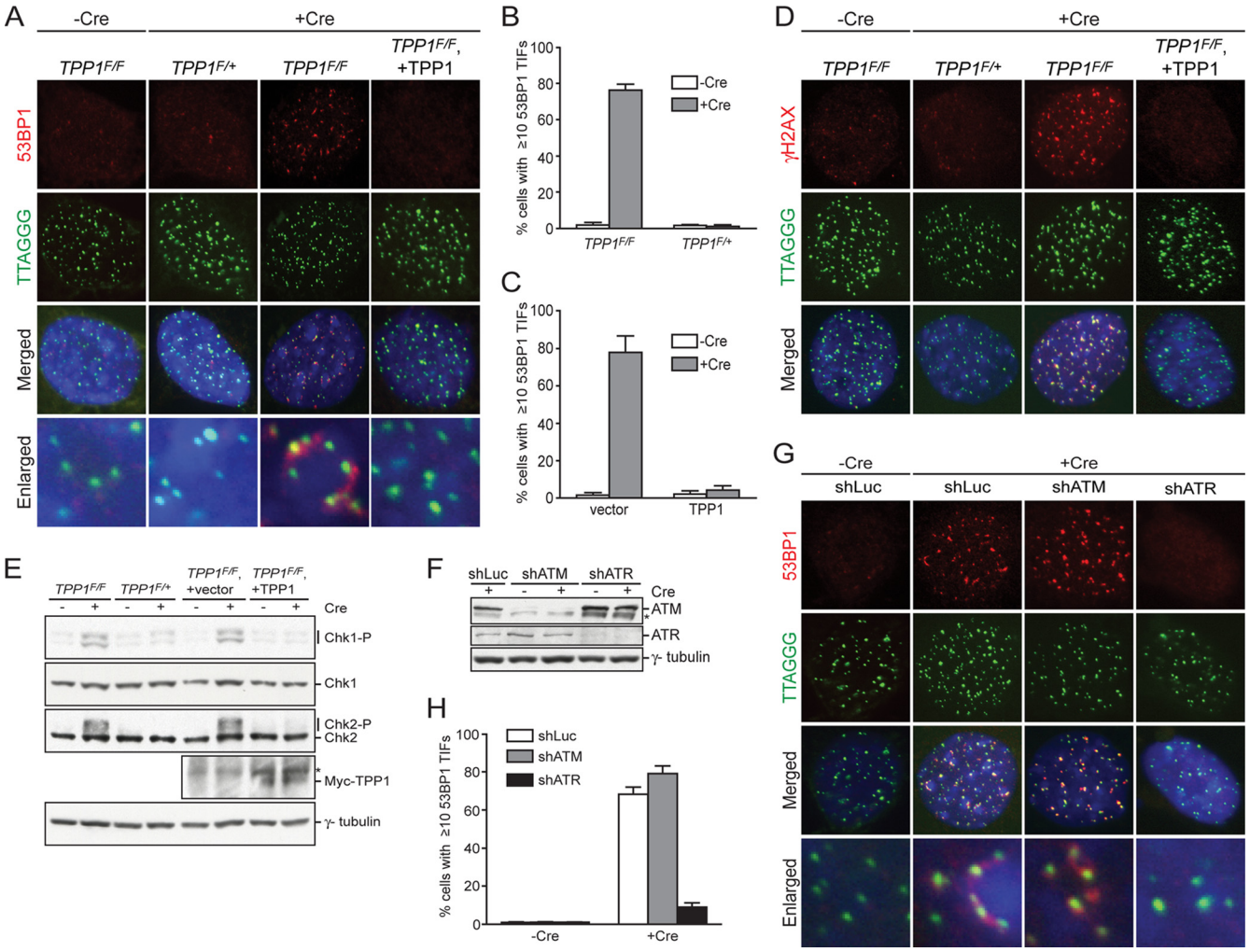


FIG. 2. ATR-dependent DNA damage signaling in *TPP1* KO cells. (A) Induction of TIFs by deletion of *TPP1*. *TPP1*$^{F/F}$ cells at 96 h after Cre (or mock) infection were analyzed using FISH for telomeres (FITC, green) and IF for 53BP1 (Alexa 555, red). (B) Quantification of the TIF response. Cells shown in panel A were scored for 10 or more telomeric 53BP1 foci. Bars show average results of three independent experiments and standard deviations. (C) Exogenous TPP1 expression represses TIF formations in *TPP1* KO cells. The TIF response was quantified as for panels A and B. (D) γH2AX TIFs induced by *TPP1* deletion. *TPP1*$^{F/F}$ cells were analyzed using FISH for telomeres (FITC, green) and IF for γH2AX (RRX, red) at the same time point as in panel A after Cre infection. (E) Loss of TPP1 induces phosphorylation of Chk1 and Chk2. The indicated cells were harvested at 96 h after Cre infection and processed for immunoblotting for the indicated proteins. Asterisk, nonspecific band. (F) Immunoblots verifying shRNA-mediated knockdown of ATM and ATR. Cells infected with the indicated shRNAs were collected and analyzed at 96 h after Hit&Run-Cre infection. (G) ATR-dependent TIF formation upon *TPP1* deletion. Cells infected with the indicated shRNAs were analyzed using FISH for telomeres (FITC, green) and IF for 53BP1 (Alexa 555, red) at the same time point as in panel F after Cre infection. (H) Quantification of the effect of ATM and ATR knockdown on the TIF response upon *TPP1* deletion. Cells were treated as for panel G and scored for 10 or more telomeric 53BP1 foci. Bars show average results of two independent experiments and standard errors of the means.

ies—53BP1 (100-304) (rabbit polyclonal; Novus Biological) and γH2AX (JBW301) (mouse monoclonal; Millipore)—were incubated in blocking solution for 1 h at room temperature, followed by three PBS washes, incubation with Rhodamine Red-X-labeled rabbit-raised secondary antibody (RRX; Jackson) or Alexa Fluor 555-labeled mouse-raised secondary antibody (Invitrogen) in blocking solution for 30 min at room temperature, and three PBS washes. Coverslips were dehydrated with 70%, 95%, and 100% ethanol and allowed to dry completely. Hybridizing solution [70% formamide, 0.5% blocking reagent (Roche), 10 mM Tris-HCl, pH 7.2, fluorescein isothiocyanate (FITC)-OO-(CCCTAAA)3 PNA probe (Applied Biosystems)] was added to each coverslip, and the coverslips were heated for 10 min at 80°C. After incubation for 2 h at room temperature, coverslips were washed twice in washing solution (70% formamide, 10 mM Tris-HCl, pH 7.2) and three times in PBS. DNA was counterstained with DAPI (4′,6-diamidino-2-phenylindole), and slides were mounted in anti-fade reagent (ProLong Gold; Invitrogen). Digital images were captured with a Zeiss Axioplan II microscope with a Hamamatsu C4742-95 camera using Improvision OpenLab software.

**Telomere overhang assay.** Telomeric overhangs were analyzed as described previously (3). Briefly, genomic DNA in plugs was digested with MboI, separated by pulsed-field gel electrophoresis, and hybridized to a nondenatured gel with a [CCCTAA]4 oligonucleotide to measure telomere overhang signals. The DNAs were denatured *in situ* with NaOH, neutralized, and rehybridized with the same probe to measure total telomeric DNA signals. The overhang signals were normalized to total telomeric DNA signals in the same lane, and these ratios were compared between samples analyzed on the same gel.

**Telomere FISH on metaphase spreads.** Cells were harvested and fixed as described previously (31). Metaphase spreads were aged overnight, and PNA-FISH was performed (19). Briefly, slides were washed in PBS once, dehydrated with 75%, 95%, and 100% ethanol, and allowed to dry up completely. Hybridizing solution [70% formamide, 0.5% blocking reagent (Roche), 10 mM Tris-

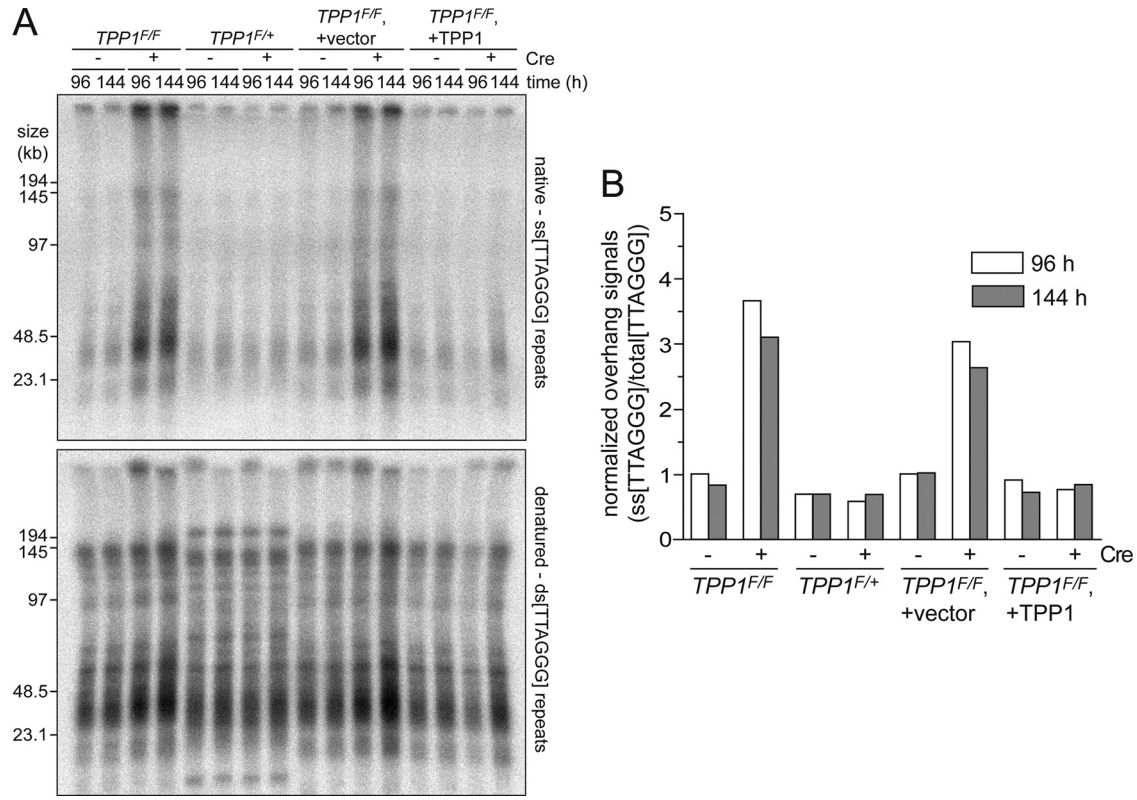


FIG. 3. TPP1 deficiency induces excess single-stranded telomeric DNA. (A) In-gel overhang assay with the indicated MEFs at the indicated time points after infection with Cre (or mock treatment). Molecular sizes are indicated in kilobases. (B) Quantification of the overhang signals of the gel shown in panel A. The single-stranded telomeric DNA signal was normalized to the double-stranded telomeric DNA signal.

HCl, pH 7.2, FITC-OO-(CCCTAAA)3 PNA probe (Applied Biosystems)] was added to slides, and the slides were heated for 3 min at 80°C. The slides were hybridized in the dark for 2 h at room temperature. The slides were washed twice in 70% formamide–10 mM Tris-HCl, pH 7.2–0.1% BSA, and three times in 10 mM Tris-HCl, pH 7.2–150 mM NaCl-0.08% Tween 20. DAPI was added to the second wash to counterstain the chromosomal DNA, and slides were mounted in anti-fade reagent (ProLong Gold; Invitrogen). Digital images were captured with a Zeiss Axioplan II microscope with a Hamamatsu C4742-95 camera using Improvision OpenLab software.

**Fluorescence-activated cell sorter (FACS) analysis.** Cells were trypsinized, suspended in medium with 10% FCS, collected by centrifugation, washed with PBS, and fixed with ice-cold 70% ethanol. Cells were resuspended in 300 μl in PBS with 5 μg propidium iodide (PI), 0.5% BSA, and 100 μg/ml RNase A. Samples were analyzed with a FACSCalibur flow cytometer (Becton Dickinson) using FlowJo.

## RESULTS AND DISCUSSION

**Conditional deletion of *TPP1*.** The *TPP1* locus on mouse chromosome 8 was modified by gene targeting, resulting in a floxed allele (Fig. 1A). The floxed allele carried two *loxP* sites in the second and eighth introns of the gene. Following Cre-mediated deletion of exons 3 to 8, the predicted protein is severely truncated, containing the N-terminal 79 amino acids of TPP1 followed by 17 out-of-frame amino acids prior to a stop codon. This truncated TPP1 lacks part of the OB fold, the POT1a/b interaction domain, the serine-rich region, and all of the TIN2 interaction domain (Fig. 1A). Crosses of $TPP1^{Del/+}$ mice generated no live-born $TPP1^{Del/Del}$ mice out of a total of 99 pups (25 expected, $\chi^2 = 34.51$, $P < 0.001$). At embryonic day 14.5, no $TPP1^{Del/Del}$ embryos were observed out of 28 examined (7 expected, $\chi^2 = 9.36$, $P < 0.01$), establishing that the $TPP1^{Del}$ allele results in early embryonic lethality when homozygous.

SV40 large-T-antigen-immortalized $TPP1^{F/F}$ and $TPP1^{F/+}$ mouse embryonic fibroblasts (MEFs) were generated from littermate E13.5 embryos derived from $TPP1^{F/+}$ intercrosses. Expression of Cre recombinase in these cells resulted in a growth defect and signs of senescence in $TPP1^{F/F}$ cells but not in $TPP1^{F/+}$ MEFs (Fig. 1B to D). The growth defect could be rescued by exogenous TPP1, indicating that it was due to deletion of the *TPP1* gene (data not shown).

The cellular and organismal lethality of *TPP1* deletion and the telomere dysfunction phenotypes described below are distinct from the milder phenotypes observed in the Acd mice (14). This result is consistent with data indicating that Acd mice contain sufficient residual TPP1 for the essential functions of TPP1 (14).

**Loss of POT1a and POT1b from chromatin and telomeres.** Deletion of *TPP1* resulted in a significant loss of POT1a and POT1b from telomeres as deduced from ChIP analysis (Fig. 1E and F). In contrast, the ChIP signals of TRF1, TRF2, Rap1, and TIN2 were not affected and these shelterin proteins remained readily detectable at telomeres by IF (data not shown). The effect of *TPP1* deletion on the localization of POT1 proteins was also observed in fractionation experiments. Whereas POT1a and POT1b are recovered in the chromatin-bound protein fraction from wild-type cells, both proteins were released from the chromatin of *TPP1*-deficient cells (Fig. 1G). As

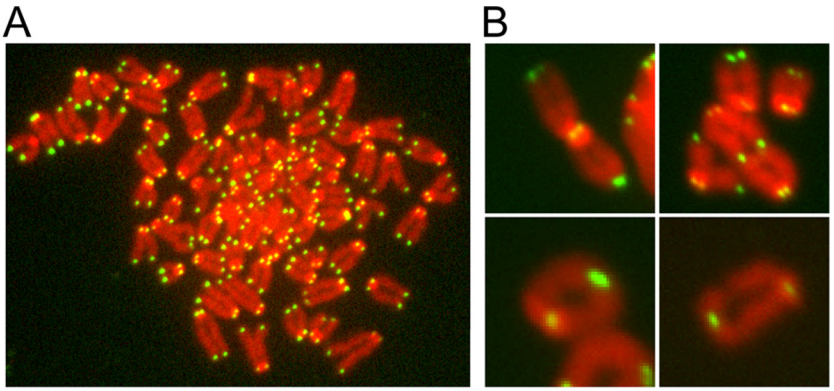


C

| | telomeres analysed | chromosome fusions +tel. signals | chromosome fusions -tel. signals | sister fusions (long arms) | multiple tel. signals |
|---|---|---|---|---|---|
| *TPP1*$^{F/F}$ | 8598 | 8 | 0 | 0 | 0 |
| *TPP1*$^{F/F}$ +Cre | 7851 | 310 (4.0%) | 32 (0.4%) | 136 (3.5%) | 16 (0.2%) |
| *TPP1*$^{F/+}$ | 7620 | 0 | 8 | 3 | 0 |
| *TPP1*$^{F/+}$ +Cre | 7794 | 4 | 0 | 0 | 4 |

FIG. 4. Sister telomere fusions and infrequent chromosome-type fusions in *TPP1* null cells. (A) Metaphase from *TPP1*$^{F/F}$ cells at 144 h after Cre infection. DNA was stained with DAPI (false colored in red). Telomere DNA was detected by FISH (FITC, green). (B) Examples of chromosome-type fusions and sister telomere fusions in *TPP1* KO cells. Experimental conditions are as for panel A. (C) Quantification of the types of telomere fusions in TPP1 null cells analyzed as for panel A. Telomere sister fusions were not scored for the short-arm telomeres because their proximity can lead to spurious coincidence of the telomeric signals.

a control, TPP1 had no effect on the fractionation behavior of TRF2, which remained in the chromatin-bound fraction upon *TPP1* deletion (Fig. 1G). Thus, TPP1 is required for the localization of POT1a and POT1b to telomeric chromatin but not for the stability of these proteins.

**ATR kinase-dependent DNA damage signaling.** *TPP1* deletion elicited a robust TIF response at chromosome ends that was suppressed by the expression of exogenous TPP1 (Fig. 2A to C). At day 4 after introduction of Cre to delete TPP1, most cells contained 53BP1 and phosphorylated H2AX at the majority of their telomeres (Fig. 2A to D).

Deletion of the POT1 proteins induces phosphorylation of Chk1 as well as Chk2 (20). The Chk1 activation is mediated by ATR signaling at telomeres lacking POT1a/b. The activation of Chk2 is likely due to secondary activation of ATM signaling after the breakage of dicentric chromosomes formed through occasional telomere fusions. This typical pattern of dual Chk1 and Chk2 phosphorylation was also observed in the *TPP1* KO setting (Fig. 2E). As with the induction of TIFs, the phosphorylation of Chk1 and Chk2 could be repressed by exogenous TPP1. Consistent with the phosphorylation of Chk1, the DNA damage signal at telomeres in *TPP1* null cells appeared to be a result of activation of the ATR kinase (Fig. 2F to H). The contribution of the ATR and ATM kinases was determined using shRNA-mediated partial depletion (Fig. 2F). Knockdown of the ATR kinase strongly attenuated the telomere damage response, whereas inhibition of the ATM kinase had no effect (Fig. 2G and H). These data suggest that deletion of *TPP1* results in the same telomere damage phenotype as loss of POT1a/b, characterized by ATR-dependent damage signaling at telomeres and activation of Chk1 and Chk2.

**Excess single-stranded telomeric DNA.** A typical phenotype of deletion of *POT1b* is the induction of excess single-stranded telomeric DNA, presumably because of deregulation of a nuclease that resects the C-rich telomeric DNA strand (11–13). In-gel hybridization to quantify the single-stranded telomeric DNA showed that this phenotype is recapitulated in the *TPP1* null cells (Fig. 3A and B). At 4 to 6 days after introduction of Cre into the *TPP1*$^{F/F}$ cells, the amount of single-stranded telomeric DNA increased 2.5- to 3.5-fold. As for the other phenotypes, this change was not observed in cells expressing exogenous TPP1, showing that the effect was due to deletion of the mouse *TPP1* gene.

**TPP1 loss recapitulates the POT1a/b DKO pattern of telomere fusions.** Deletion of *TPP1* resulted in occasional telomeric fusion events detectable in metaphase spreads. Although the majority of chromosomes appeared normal (Fig. 4A), *TPP1*-deficient cells showed a low number of chromosome-type fusions with telomeric signals at the fusion points (Fig. 4B and C). In addition, the cells contained fusions between sister telomeres (Fig. 4B and C). Both types were present at approximately the same low frequency, involving 3 to 4% of telomeres. Chromatid-type fusions involving telomeres from different chromosomes were not observed. In addition, the chromosome-type fusions rarely involved more than two chromosomes. The low frequency of telomere fusions, the paucity of chromosome trains, and the absence of fusions between nonsister telomeres are typical of the POT1a/b DKO pheno-

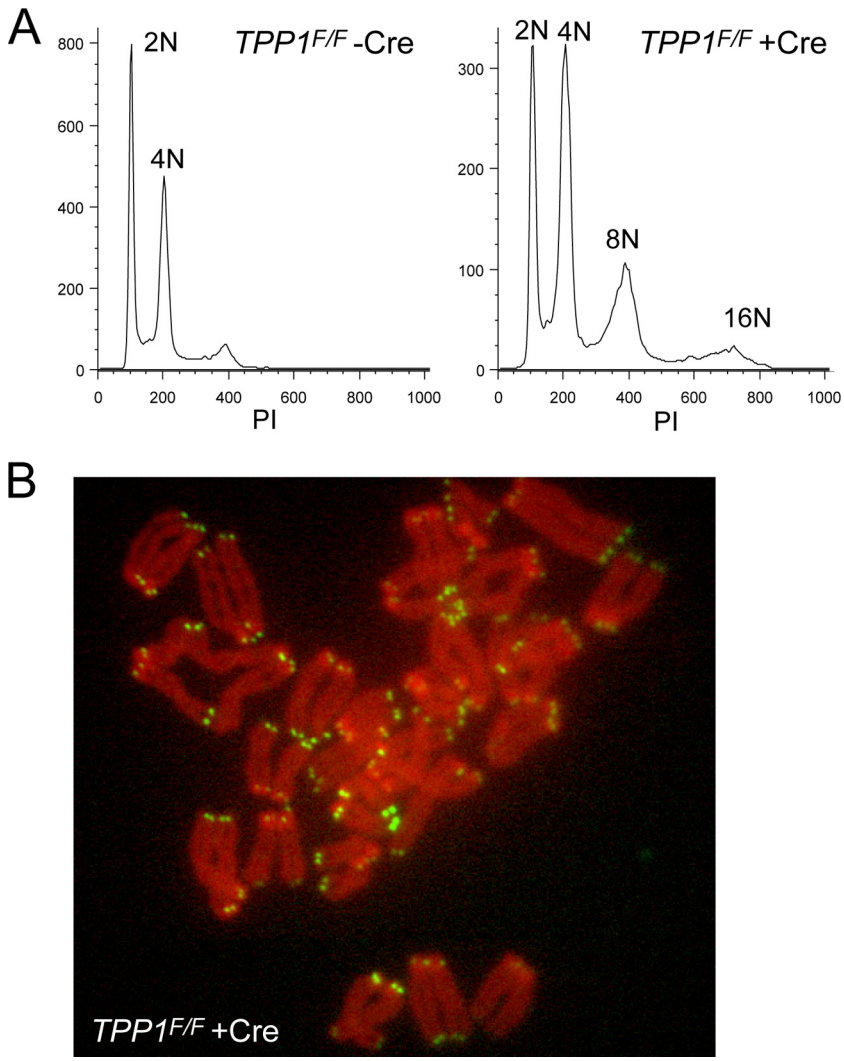


FIG. 5. The deletion of *TPP1* induces endoreduplication. (A) DNA profiles of $TPP^{F/F}$ cells before and after Cre. Cells were harvested and fixed at 5 days after Cre infection. DNA content was analyzed by FACS (PI staining). Sub-$G_1$ cells are not shown. (B) Telomere FISH on a metaphase spread derived from *TPP1* KO cells showing diplochromosomes.

type. In contrast, the loss of TRF2 results in fusions that are 10-fold more frequent, involve multiple chromosomes, and rarely join sister telomeres. Other aberrations, including signal-free ends, fragile telomeres, and TDMs (telomeric DNA containing double minutes), were not induced by *TPP1* deletion. However, TPP1 loss did result in a few chromosome-type fusions lacking telomeric signals and chromosomes with multiple telomeric signals (Fig. 4C), but these aberrant structures could be a secondary consequence of breakage-fusion bridge cycles initiated by the chromosome-type fusions and the sister fusions. We conclude that the pattern of chromosomal abnormalities in *TPP1*-deficient cells closely resembles that of POT1a/b DKO cells.

**Endoreduplication in *TPP1* KO cells.** A striking phenotype of *TPP1*-deficient cells was endoreduplication. At day 5 after the introduction of Cre, $TPP1^{F/F}$ cells showed aberrant FACS profiles with a substantial fraction of cells with >4 N genome content (Fig. 5A). The peaks in the FACS profiles were discrete, indicating whole genome duplications. This endoreduplication phenotype is also observed in POT1a/b DKO cells, where it is accompanied by metaphase spreads containing diplo- and quadruplochromosomes and interphase nuclei containing supernumerary telomeres that are often clustered (12). Metaphases with diplochromosomes also occurred occasionally in the *TPP1* knockout cells (Fig. 5B) although they were rare (~5%). A substantial fraction of the interphase nuclei (>30%) showed supernumerary telomeres that were often clustered (Fig. 2A, D, and G). Thus, the endoreduplication phenotype of *TPP1* KO cells is similar to that of POT1a/b loss.

**Conclusions.** These data establish that the phenotypes associated with the removal of TPP1 from mouse telomeres recapitulate the consequences of deletion of POT1a and POT1b. TPP1-deficient cells show a combination of specific indices of the type of telomere dysfunction induced by the loss of both POT1 proteins: ATR-dependent DNA damage signaling with accompanying phosphorylation of Chk1 and Chk2, a low level of telomere fusions that often involve sister telomeres, a severalfold increase in the abundance of the single-stranded telo-

meric DNA, and frequent endoreduplication. Telomere dysfunction phenotypes that are indicative of impaired function of TRF1 or TRF2 were not observed. In particular, TPP1-deficient cells showed neither the fragile telomere phenotype specific to TRF1 loss nor the ATM-dependent DNA damage signaling typical of TRF2 loss. All phenotypes induced by the deletion of *TPP1* were consistent with the consequences of POT1a/b loss. We conclude, therefore, that TPP1 is dedicated to a telomeric function and that its function is executed in conjunction with its interacting partners POT1a and POT1b. The data also show that POT1a and POT1b are dependent on TPP1 for their localization at telomeres. Both proteins are incapable of associating with chromatin in the absence of TPP1, and telomeric ChIP suggests that they are absent from telomeres in TPP1-deficient cells. Thus, mammalian POT1, like its ciliate counterparts, functions as a heterodimer with TPP1.

## ACKNOWLEDGMENTS

We acknowledge Elizabeth Hughes, Yun Yan Qu, Keith Childs, Galina Gavrillina, and Debra Vanheyningen for preparation of gene-targeted mice and the Transgenic Animal Model Core of the University of Michigan's Biomedical Research Core Facilities. We thank Devon White for expert mouse husbandry, Eros Lazzerini Denchi for his contributions to generating the TPP1-targeted MEFs, and Hiro Takai for experimental advice.

Core support was provided by the University of Michigan Cancer Center, NIH grant no. CA46592, and the University of Michigan Center for Organogenesis. This work was supported by grants from the NIH to T.D.L. (GM049046 and AG016642) and to C.E.K. (HD058606). T.K. was supported by a postdoctoral fellowship from the Toyobo Biotechnology Foundation.

## REFERENCES

1. **Barrientos, K. S., M. F. Kendellen, B. D. Freibaum, B. N. Armbruster, K. T. Etheridge, and C. M. Counter.** 2008. Distinct functions of POT1 at telomeres. Mol. Cell. Biol. **28:**5251–5264.
2. **Baumann, P., and T. R. Cech.** 2001. Pot1, the putative telomere end-binding protein in fission yeast and humans. Science **292:**1171–1175.
3. **Celli, G., and T. de Lange.** 2005. DNA processing not required for ATM-mediated telomere damage response after TRF2 deletion. Nat. Cell Biol. **7:**712–718.
4. **Chen, L. Y., D. Liu, and Z. Songyang.** 2007. Telomere maintenance through spatial control of telomeric proteins. Mol. Cell. Biol. **27:**5898–5909.
5. **de Lange, T.** 2005. Shelterin: the protein complex that shapes and safeguards human telomeres. Genes Dev. **19:**2100–2110.
6. **de Lange, T.** 2009. How telomeres solve the end-protection problem. Science **326:**948–952.
7. **Dimitrova, N., and T. de Lange.** 2006. MDC1 accelerates nonhomologous end-joining of dysfunctional telomeres. Genes Dev. **20:**3238–3243.
8. **Dimri, G. P., X. Lee, G. Basile, M. Acosta, G. Scott, C. Roskelley, E. E. Medrano, M. Linskens, I. Rubelj, O. Pereira-Smith, N. Oeacicjem, and J. Campisi.** 1995. A biomarker that identifies senescent human cells in culture and in aging skin in vivo. Proc. Natl. Acad. Sci. U. S. A. **92:**9363–9367.
9. **Else, T., B. K. Theisen, Y. Wu, J. E. Hutz, C. E. Keegan, G. D. Hammer, and D. O. Ferguson.** 2007. Tpp1/Acd maintains genomic stability through a complex role in telomere protection. Chromosome Res. **15:**1001–1013.
10. **George, S. H., M. Gertsenstein, K. Vintersten, E. Korets-Smith, J. Murphy, M. E. Stevens, J. J. Haigh, and A. Nagy.** 2007. Developmental and adult phenotyping directly from mutant embryonic stem cells. Proc. Natl. Acad. Sci. U. S. A. **104:**4455–4460.
11. **He, H., Y. Wang, X. Guo, S. Ramchandani, J. Ma, M. F. Shen, D. A. Garcia, Y. Deng, A. S. Multani, M. J. You, and S. Chang.** 2009. Pot1b deletion and telomerase haploinsufficiency in mice initiate an ATR-dependent DNA damage response and elicit phenotypes resembling dyskeratosis congenita. Mol. Cell. Biol. **29:**229–240.
12. **Hockemeyer, D., J. P. Daniels, H. Takai, and T. de Lange.** 2006. Recent expansion of the telomeric complex in rodents: two distinct POT1 proteins protect mouse telomeres. Cell **126:**63–77.
13. **Hockemeyer, D., W. Palm, R. C. Wang, S. S. Couto, and T. de Lange.** 2008. Engineered telomere degradation models dyskeratosis congenita. Genes Dev. **22:**1773–1785.
14. **Hockemeyer, D., W. Palm, T. Else, J. P. Daniels, K. K. Takai, J. Z. Ye, C. E. Keegan, T. de Lange, and G. D. Hammer.** 2007. Telomere protection by mammalian POT1 requires interaction with TPP1. Nat. Struct. Mol. Biol. **14:**754–761.
15. **Houghtaling, B. R., L. Cuttonaro, W. Chang, and S. Smith.** 2004. A dynamic molecular link between the telomere length regulator TRF1 and the chromosome end protector TRF2. Curr. Biol. **14:**1621–1631.
16. **Karlseder, J., D. Broccoli, Y. Dai, S. Hardy, and T. de Lange.** 1999. p53- and ATM-dependent apoptosis induced by telomeres lacking TRF2. Science **283:**1321–1325.
17. **Kendall, S. K., L. C. Samuelson, T. L. Saunders, R. I. Wood, and S. A. Camper.** 1995. Targeted disruption of the pituitary glycoprotein hormone alpha-subunit produces hypogonadal and hypothyroid mice. Genes Dev. **9:**2007–2019.
18. **Konishi, A., and T. de Lange.** 2008. Cell cycle control of telomere protection and NHEJ revealed by a ts mutation in the DNA-binding domain of TRF2. Genes Dev. **22:**1221–1230.
19. **Lansdorp, P. M., N. P. Verwoerd, F. M. van de Rijke, V. Dragowska, M. T. Little, R. W. Dirks, A. K. Raap, and H. J. Tanke.** 1996. Heterogeneity in telomere length of human chromosomes. Hum. Mol. Genet. **5:**685–691.
20. **Lazzerini Denchi, E., and T. de Lange.** 2007. Protection of telomeres through independent control of ATM and ATR by TRF2 and POT1. Nature **448:**1068–1071.
21. **Liu, D., A. Safari, M. S. O'Connor, D. W. Chan, A. Laegeler, J. Qin, and Z. Songyang.** 2004. PTOP interacts with POT1 and regulates its localization to telomeres. Nat. Cell Biol. **6:**673–680.
22. **Liu, P., N. A. Jenkins, and N. G. Copeland.** 2003. A highly efficient recombineering-based method for generating conditional knockout mutations. Genome Res. **13:**476–484.
23. **Loayza, D., and T. de Lange.** 2003. POT1 as a terminal transducer of TRF1 telomere length control. Nature **423:**1013–1018.
24. **Mendez, J., and B. Stillman.** 2000. Chromatin association of human origin recognition complex, Cdc6, and minichromosome maintenance proteins during the cell cycle: assembly of prereplication complexes in late mitosis. Mol. Cell. Biol. **20:**8602–8612.
25. **O'Connor, M. S., A. Safari, H. Xin, D. Liu, and Z. Songyang.** 2006. A critical role for TPP1 and TIN2 interaction in high-order telomeric complex assembly. Proc. Natl. Acad. Sci. U. S. A. **103:**11874–11879.
26. **Palm, W., D. Hockemeyer, T. Kibe, and T. de Lange.** 2009. Functional dissection of human and mouse POT1 proteins. Mol. Cell. Biol. **29:**471–482.
27. **Rodriguez, C. I., F. Buchholz, J. Galloway, R. Sequerra, J. Kasper, R. Ayala, A. F. Stewart, and S. M. Dymecki.** 2000. High-efficiency deleter mice show that FLPe is an alternative to Cre-loxP. Nat. Genet. **25:**139–140. (Letter.)
28. **Sfeir, A., S. T. Kosiyatrakul, D. Hockemeyer, S. L. MacRae, J. Karlseder, C. L. Schildkraut, and T. de Lange.** 2009. Mammalian telomeres resemble fragile sites and require TRF1 for efficient replication. Cell **138:**90–103.
29. **Silver, D. P., and D. M. Livingston.** 2001. Self-excising retroviral vectors encoding the Cre recombinase overcome Cre-mediated cellular toxicity. Mol. Cell **8:**233–243.
30. **Takai, K. K., S. M. Hooper, S. L. Blackwood, R. Gandhi, and T. de Lange.** 2010. In vivo stoichiometry of shelterin components. J. Biol. Chem. **285:**1457–1467.
31. **van Steensel, B., A. Smogorzewska, and T. de Lange.** 1998. TRF2 protects human telomeres from end-to-end fusions. Cell **92:**401–413.
32. **Wang, F., E. R. Podell, A. J. Zaug, Y. Yang, P. Baciu, T. R. Cech, and M. Lei.** 2007. The POT1-TPP1 telomere complex is a telomerase processivity factor. Nature **445:**506–510.
33. **Xin, H., D. Liu, M. Wan, A. Safari, H. Kim, W. Sun, M. S. O'Connor, and Z. Songyang.** 2007. TPP1 is a homologue of ciliate TEBP-beta and interacts with POT1 to recruit telomerase. Nature **445:**559–562.
34. **Yang, Q., Y. L. Zheng, and C. C. Harris.** 2005. POT1 and TRF2 cooperate to maintain telomeric integrity. Mol. Cell. Biol. **25:**1070–1080.
35. **Ye, J. Z., D. Hockemeyer, A. N. Krutchinsky, D. Loayza, S. M. Hooper, B. T. Chait, and T. de Lange.** 2004. POT1-interacting protein PIP1: a telomere length regulator that recruits POT1 to the TIN2/TRF1 complex. Genes Dev. **18:**1649–1654.